

Asymmetric stochastic resonance under non-Gaussian colored noise and time-delayed feedback

Ting-Ting Shi(石婷婷), Xue-Mei Xu(许雪梅), Ke-Hui Sun(孙克辉), Yi-Peng Ding(丁一鹏), Guo-Wei Huang(黄国伟)

Citation: Chin. Phys. B . 2020, 29(5): 050501 . **doi:** 10.1088/1674-1056/ab7e9f
Journal homepage: http://cpb.iphy.ac.cn; http://iopscience.iop.org/cpb

What follows is a list of articles you may be interested in

Ergodicity recovery of random walk in heterogeneous disordered media

Liang Luo(罗亮), Ming Yi(易鸣)
Chin. Phys. B . 2020, 29(5): 050503 . **doi:** 10.1088/1674-1056/ab8212

Novel Woods-Saxon stochastic resonance system for weak signal detection

Yong-Hui Zhou(周永辉), Xue-Mei Xu(许雪梅), Lin-Zi Yin(尹林子), Yi-Peng Ding(丁一鹏), Jia-Feng Ding(丁家峰), Ke-Hui Sun(孙克辉)
Chin. Phys. B . 2020, 29(4): 040503 . **doi:** 10.1088/1674-1056/ab75ca

Ratchet transport of overdamped particles in superimposed driven lattices

Shu-Na Huang(黄淑娜), Wei-Jing Zhu(朱薇静), Xiao-Qun Huang(黄小群), Bao-Quan Ai(艾保全), Feng-Guo Li(李丰果)
Chin. Phys. B . 2019, 28(4): 040502 . **doi:** 10.1088/1674-1056/28/4/040502

Transport of velocity alignment particles in random obstacles

Wei-jing Zhu(朱薇静), Xiao-qun Huang(黄小群), Bao-quan Ai(艾保全)
Chin. Phys. B . 2018, 27(8): 080504 . **doi:** 10.1088/1674-1056/27/8/080504

Control of the patterns by using time-delayed feedback near the codimension-three Turing–Hopf–Wave bifurcations

Wang Hui-Juan, Wang Yong-Jie, Ren Zhi
Chin. Phys. B . 2013, 22(12): 120503 . **doi:** 10.1088/1674-1056/22/12/120503

Asymmetric stochastic resonance under non-Gaussian colored noise and time-delayed feedback*

Ting-Ting Shi(石婷婷), Xue-Mei Xu(许雪梅)†, Ke-Hui Sun(孙克辉), Yi-Peng Ding(丁一鹏), and Guo-Wei Huang(黄国伟)

School of Physics and Electronics, Central South University, Changsha 410083, *China*

(Received 19 February 2020; revised manuscript received 4 March 2020; accepted manuscript online 11 March 2020)

Based on adiabatic approximation theory, in this paper we study the asymmetric stochastic resonance system with time-delayed feedback driven by non-Gaussian colored noise. The analytical expressions of the mean first-passage time (MFPT) and output signal-to-noise ratio (SNR) are derived by using a path integral approach, unified colored-noise approximation (UCNA), and small delay approximation. The effects of time-delayed feedback and non-Gaussian colored noise on the output SNR are analyzed. Moreover, three types of asymmetric potential function characteristics are thoroughly discussed. And they are well-depth asymmetry (DASR), well-width asymmetry (WASR), and synchronous action of well-depth and well-width asymmetry (DWASR), respectively. The conclusion of this paper is that the time-delayed feedback can suppress SR, however, the non-Gaussian noise deviation parameter has the opposite effect. Moreover, the correlation time plays a significant role in improving SNR, and the SNR of asymmetric stochastic resonance is higher than that of symmetric stochastic resonance. Our experiments demonstrate that the appropriate parameters can make the asymmetric stochastic resonance perform better to detect weak signals than the symmetric stochastic resonance, in which no matter whether these signals have low frequency or high frequency, accompanied by strong or weak noise.

Keywords: asymmetric stochastic resonance, time-delayed feedback, non-Gaussian colored noise,weak signal detection

PACS: 05.40.–a, 02.50.–r **DOI:** 10.1088/1674-1056/ab7e9f

1. Introduction

Weak signal detection is a cutting-edged methodology in which the modern electronics and information-processing methods are used to detect weak signals in strong background noise environment.[1–5] Since the 1940s, weak signal detection has been widely used in relevant theoretical researches and practical applications. As a new method different from the previous weak signal detection, the stochastic resonance (SR) has made great progress since the quaternary global meteorological glaciers was studied by Benzi *et al.* in 1981.[6] The SR studies mainly focus on bistable stochastic resonance but also including monostable stochastic resonance[7–9] and tristable stochastic resonance.[10–12] The SR of this paper is referred to as the bistable stochastic resonance.

The previous studies of SR were generally based on the symmetric potential function,[13–15] but there were few studies based on asymmetric potential functions, and most of them are asymmetric systems in real natural systems. So studying asymmetric systems is another key point in the development of SR theory. The traditional SR theory is mainly applied to the researches of the symmetric potential function. And then, Wio and Bouzat[16] extended the adiabatic approximation theory to the asymmetric potential function. In the adiabatic approximation theory, a transition between two wells is the reciprocal of the MFPT. Subsequently, some researchers studied the effect of asymmetry on the SR generated under multiplicative noise. Li[17] found that the asymmetry is negatively correlated with SR. Owing to the fact that different physical systems are affected by different noise sources and Gaussian white noise does not exist in nature, it is especially necessary to study the SR driven by different noises. Fuentes *et al.*[18] investigated the effect of non-Gaussian colored noise on SR phenomenon. The path integral approach[19–23] and the UCNA[24] are used to convert the non-Gaussian colored noise into Gaussian white noise, thus obtaining a Fokker–Planck equation and an output SNR analytical expression. Wang *et al.*[25] discussed in detail the effect of the correlation between two multiplicative noises and an additive noise on the MFPT and found that it possesses rich transition phenomena. Dybiech and Nowak[26] studied the generic double-well potential model perturbed by the alpha-stable Lévy-type noises. To freely adjust the width and depth of the barrier, Liu and Cao[27] designed a piecewise potential function to analyze the effect of the asymmetry of the well on the SNR in the background of non-Gaussian colored noise.

Since time lags are widespread in nature, the study of SR with time-delayed feedback conforms to the developing trend.[28–34] Shi *et al.*[28] derived the expression of the steady-state probability density function (SPD) and SNR of SR with time-delayed feedback, suggesting that the delay time and feedback strength of the time-delayed term can enhance the SNR. Introducing time-delayed terms into the potential func-

*Project supported by the National Natural Science Foundation of China (Grant No. 60551002) and the Natural Science Foundation of Hunan Province, China (Grant No. 2018JJ3680).

†Corresponding author. E-mail: xuxuemei999@126.com

© 2020 Chinese Physical Society and IOP Publishing Ltd

tion can reduce the SNR, but the degradation reaction has the opposite effect.[29] According to the time-delayed feedback and Gaussian white noise, Tang *et al.*[30] proposed an asymmetric SR detection method. This method overcomes the shortcomings of the traditional SR, which has a long convergence time and tends to easily fall into local optimization. Therefore, the detection of weak fault features is improved. Liu and Wang[31] discussed the effects of additive white Gaussian noise and time-delayed feedback on the SR under three asymmetric potential functions. Tan *et al.*[32] investigated the effects of additive colored noise and time-delayed feedback on two asymmetric systems. For asymmetric systems, they analyzed the effects of noise and time-delayed feedback on SR performance in detail, respectively. However, the effect of asymmetric SR under the combination of non-Gaussian colored noise and time-delayed feedback can be further studied.

In this paper, we study an SR with time-delayed feedback in the context of non-Gaussian colored noise. The rest of this paper is organized as follows. In Section 2, we introduce the potential function model of the system, and on this basis, derive the output SNR expression of the system. Meanwhile, we analyze in detail the effects of non-Gaussian colored noise and time-delayed feedback on the three asymmetric potential functions. In Section 3, we introduce particle swarm optimization and gives some experiments to detect low-frequency and high-frequency weak signals that are submerged by non-Gaussian colored noise. Finally, some conclusions are drawn from the present study in Section 4.

2. Asymmetric bistable stochastic resonance

2.1. Asymmetric bistable potential function

The classical bistable stochastic resonance (CSR) model can be represented by the Langevin equation

$$\frac{\mathrm{d}x}{\mathrm{d}t} = -\frac{\mathrm{d}U_i(x)}{\mathrm{d}t} + A\cos(2\pi f t) + \Gamma(t), \tag{1}$$

where $U_i(x)$ is the bistable potential function, A and f are the amplitude and frequency of the periodic signal, respectively, and $\Gamma(t)$ is the noise. In order to study the relationship between asymmetric structure and SR, the asymmetry factor $\alpha\,(\alpha>0)$ is introduced to construct the bistable potential function[27,31,32] as follows:

$$U_i(x) = \begin{cases} -\dfrac{a}{2}x^2 + \dfrac{b}{4}x^4, & x \geqslant 0, \\ -\dfrac{a}{2}A_i x^2 + \dfrac{b}{4}B_i x^4, & x < 0, \end{cases} \tag{2}$$

where a and b are the system parameters and $a,\, b>0$. When $i=1,2,3$, as shown in Fig. 1, the potential function $U_i(x)$ is divided into three cases: the barrier height and the well spacing of the right potential well are $\Delta U_+ = a^2/4b$ and $\Delta L_+ = \sqrt{a/b}$, respectively, independent of the asymmetry factor. However, the left potential well is different. Figure 1(a) shows the DASR $U_1(x)$ with $A_1 = B_1 = \alpha$, and the barrier height of the left potential well is $\alpha a^2/4b$ and increases as α increases, when a and b are both set to be fixed values. The well spacing is $\sqrt{a/b}$ and keeps unchanged. Figure 1(b) shows the WASR $U_2(x)$ of $A_2 = 1/\alpha^2, B_2 = 1/\alpha^4$. Contrary to $U_1(x)$, the barrier height of the left potential well $\left(a^2/4b\right)$ of $U_2(x)$ does not change with α, but the well spacing $\left(\alpha\sqrt{a/b}\right)$ rises. Figure 1(c) shows the DWASR $U_3(x)$ of $A_3 = 1$, $B_3 = 1/\alpha^2$. Combining the above two cases, the barrier height $\alpha^2 a^2/4b$ and the well spacing $\alpha\sqrt{a/b}$ of the left potential well of $U_3(x)$ decrease with the decrease of α. The potential function can systematically investigate the asymmetric SR through the above analysis.

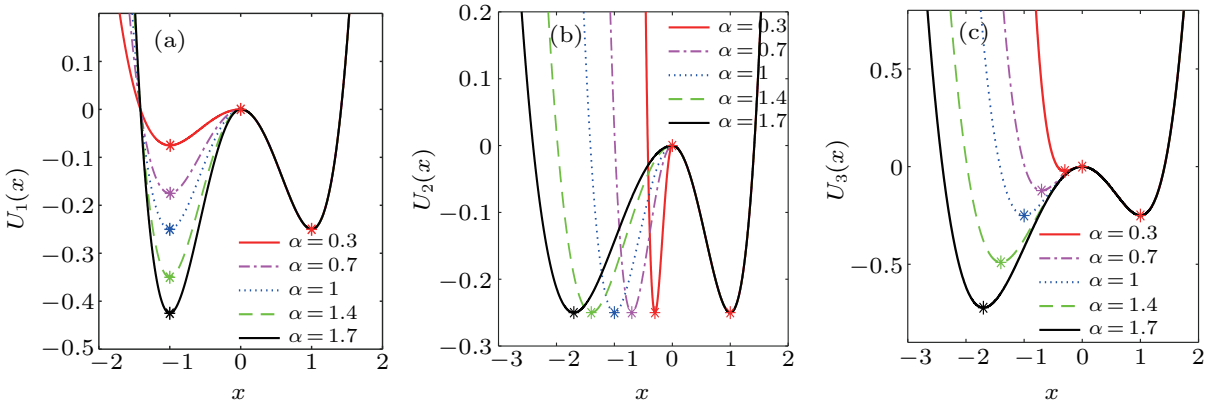


Fig. 1. Three kinds of asymmetric bistable potential functions with different asymmetric factors where $a=b=1$: (a) DASR, (b) WASR, (c) DWASR.

2.2. SNR of asymmetric bistable system

Based on the asymmetric bistable potential function of the previous section, adding the non-Gaussian colored noise and time-delayed terms, the Langevin equation can be written as follows:

$$\frac{\mathrm{d}x}{\mathrm{d}t} = -\frac{\mathrm{d}U_i(x)}{\mathrm{d}t} + kx(t-\sigma) + A\cos(\omega t) + g(x)\Gamma(t), \tag{3}$$

where k and σ are the time-delay strength and delay time of the time-delayed term, $\Gamma(t)$ represents the non-Gaussian colored noise with the following statistical properties:[35]

$$\langle \Gamma(t) \rangle = 0, \tag{4}$$

$$\langle \Gamma^2(t) \rangle = \begin{cases} \dfrac{2D}{\tau(5-3q)}, & q \in \left(-\infty, \dfrac{5}{3}\right), \\ \infty, & q \in \left[\dfrac{5}{3}, 3\right), \end{cases} \tag{5}$$

$$\frac{\mathrm{d}\Gamma(t)}{\mathrm{d}t} = -\frac{1}{\tau}\frac{\mathrm{d}}{\mathrm{d}\Gamma}\Upsilon_{\mathrm{q}}(\Gamma) + \frac{1}{\tau}\eta(t), \tag{6}$$

$$\Upsilon_{\mathrm{q}}(\Gamma) = \frac{D}{\tau(q-1)} \ln\left[1 + \frac{\tau}{D}(q-1)\frac{\Gamma^2}{2}\right]. \tag{7}$$

The parameter τ denotes the correlation time of the non-Gaussian noise and q is a measure of deviation of the non-Gaussian noise $\Gamma(t)$ from the Gaussian distribution. When parameter $q \neq 1$, $\Gamma(t)$ is the non-Gaussian noise. Otherwise, the $\Gamma(t)$ becomes the Gaussian colored noise with the correlation time τ and the noise intensity D. If $\tau = 0$, $\Gamma(t)$ is reduced to white noise, $\eta(t)$ is the Gaussian white noise ($\langle \eta(t) \rangle = 0, \langle \eta(t)\eta(t') \rangle = 2D\delta(t-t')$), and D is the noise intensity. The path integral approach[19,35] is used to convert the non-Gaussian colored noise $\Gamma(t)$ into a Gaussian colored noise with effective noise correlation time τ_0 and effective noise intensity D_0 when $|q-1| \ll 1$,

$$\tau_0 = \frac{2(2-q)}{5-3q}\tau, \tag{8}$$

$$D_0 = \left[\frac{2(2-q)}{5-3q}\right]^2 D. \tag{9}$$

$\Gamma(t)$ can be written as

$$\frac{\mathrm{d}\Gamma(t)}{\mathrm{d}t} = -\frac{\Gamma}{\tau_0} + \frac{1}{\tau_0}\eta_0(t), \tag{10}$$

where $\eta_0(t)$ is the Gaussian white noise with $\langle \eta_0(t) \rangle = 0$ and $\langle \eta_0(t)\eta_0(t') \rangle = 2D_0\delta(t-t')$.

Applying the UCNA[24] to Eq. (3), the Gaussian colored noise can be approximated by the Gaussian white noise $\Gamma_0(t)$ ($\langle \Gamma_0(t)\Gamma_0(t') \rangle = 2\delta(t)$). Assuming $g(x) = 1$ and $x(t-\sigma) = x_\sigma$, equation (3) can be ameliorated as

$$\frac{\mathrm{d}x}{\mathrm{d}t} = h(x, x_\sigma) + f(x)\Gamma_0(t), \tag{11}$$

$$h(x, x_\sigma) = \frac{-U_i'(x) + kx(t-\sigma) + A\cos(\omega t)}{Q(x, \tau_0)}, \tag{12}$$

$$f(x) = \frac{\sqrt{D_0}}{Q(x, \tau_0)}, \tag{13}$$

$$Q(x, \tau_0) = \begin{cases} 1 - \tau_0\left(a - 3bx^2 + k\right), & x \geqslant 0, \\ 1 - \tau_0\left(aA_i - 3bB_i x^2 + k\right), & x < 0. \end{cases} \tag{14}$$

The non-Gaussian noise in Eq. (3) has been simplified into Gaussian white noise with Markov property in Eq. (11). Next, the one-dimensional Markovian process is obtained by using the small delay approximation as follows:[36,37]

$$\frac{\mathrm{d}x}{\mathrm{d}t} = H(x) + F(x)\Gamma_0(t), \tag{15}$$

$$H(x) = h(x, x_\sigma) I(x, \sigma), \tag{16}$$

$$F(x) = f(x) I(x, \sigma), \tag{17}$$

$$I(x, \sigma) = \begin{cases} 1 - \dfrac{k\sigma}{1 - \tau_0(a - 3bx^2 + k)}, & x \geqslant 0, \\ 1 - \dfrac{k\sigma}{1 - \tau_0(aA_i - 3bB_i x^2 + k)}, & x < 0. \end{cases} \tag{18}$$

We obtain the Fokker–Planck equation, writing it as

$$\frac{\partial P(x,t)}{\partial t} = -\frac{\partial}{\partial t}[L(x)P(x,t)] + \frac{\partial^2}{\partial x^2}[M(x)P(x,t)], \tag{19}$$

$$L(x) = H(x) + F(x)F'(x), \tag{20}$$

$$M(x) = F^2(x), \tag{21}$$

where $L(x)$ is the drift coefficient and $M(x)$ is the diffusion coefficient. So, the analytical expression of the SPD is

$$P_{\mathrm{st}}(x) = \frac{N}{M(x)} \exp[-\psi(x)], \tag{22}$$

where N is the normalization factor, $\psi(x)$ denotes the general potential function of the asymmetric bistable system which is expressed as

$$\psi(x) = -\int \frac{L(x)}{M(x)}\mathrm{d}x, = \begin{cases} \dfrac{z_1}{4D_0} + \dfrac{z_2}{6D_0\tau_0} - \dfrac{z_3}{18bD_0\tau_0^2} \\ -\dfrac{A\cos(\omega t)}{D_0}(z_4 + z_5) - z_6, \quad x \geqslant 0, \\ \dfrac{j_1}{4D_0} + \dfrac{j_2}{6D_0\tau_0} - \dfrac{j_3}{18bB_iD_0\tau_0^2} \\ -\dfrac{A\cos(\omega t)}{D_0}(j_4 + j_5) - j_6, \quad x < 0, \end{cases} \tag{23}$$

where z_1–z_6 and j_1–j_6 can be consulted in Appendix A.

After analysis, the MFPT[19] is obtained as follows:

$$\mathrm{MFPT}_{\pm} = \frac{2\pi}{\sqrt{\left|U_i''(X_\pm)U_i''(X_0)\right|}} \exp\left(\psi(X_0) - \psi(X_\pm)\right), \tag{24}$$

where MFPT represents the average time for the SR system to transform between two states under the action of noise. In the bistable system, the transition rates $W_\pm(t)$ are inversely related to the MFPT

$$W_\pm(t) = \frac{1}{\mathrm{MFPT}_\pm}. \tag{25}$$

Using the adiabatic approximation theory, we expand transition rates $W_\pm(t)$ up to the first order of $A\cos(\omega t)$

$$\begin{cases} W_+(t) = \mu_1 - \lambda_1 A\cos(\omega t) + o(t), \\ W_-(t) = \mu_2 + \lambda_2 A\cos(\omega t) + o(t), \end{cases} \tag{26}$$

where

$$\mu_1 = W_+(t)|_{A\cos(\omega t)=0} = \frac{a}{\sqrt{2\pi}}\exp\{c_1 - c_2 + c_3 + c_4\}, \quad (27)$$

$$\lambda_1 = -\frac{\mathrm{d}W_+(t)}{\mathrm{d}[A\cos(\omega t)]}\Big|_{A\cos(\omega t)=0} = \frac{a(3q-5)^2(c_5+c_6)}{4\sqrt{2}\pi D(q-2)^2}\exp\{c_1 - c_2 + c_3 + c_4\}, \quad (28)$$

$$\mu_2 = W_-(t)|_{A\cos(\omega t)=0} = \frac{a\sqrt{A_i}}{\sqrt{2\pi}}\exp\{e_1 - e_2 + e_3 + e_4\}, \quad (29)$$

$$\lambda_2 = -\frac{\mathrm{d}W_-(t)}{\mathrm{d}[A\cos(\omega t)]}\Big|_{A\cos(\omega t)=0} = \frac{a\sqrt{A_i}(3q-5)^2(e_5+e_6)}{4\sqrt{2}\pi D(q-2)^2}\exp\{e_1 - e_2 + e_3 + e_4\}, \quad (30)$$

where c_1–c_6 and e_1–e_6 are listed in Appendix A.

Therefore, the output SNR of the asymmetric SR with non-Gaussian colored noise and time-delayed feedback can be deduced as follows:

$$\mathrm{SNR} = \frac{\pi A^2(\mu_1\lambda_2 + \mu_2\lambda_1)^2}{4\mu_1\mu_2(\mu_1+\mu_2)}. \quad (31)$$

2.3. Effect of asymmetric SR with time-delayed feedback subjected to non-Gaussian colored noise

To analyze and compare the effects of non-Gaussian colored noise and time-delay terms on the SNR between the asymmetric SR system and symmetric SR system, the system parameters $a = b = 1$, and $A = 0.5$ are selected.

Figures 2–4 show the SNR diagrams of DASR, WASR, and DWASR, respectively, where each panel (a) shows a two-dimensional graph, and each panel (b) displays a three-dimensional graph. In this case, the asymmetry factor α is a independent variable, and the SNR is a dependent variable. These three graphs have the similar change trends. When the other parameters are fixed, the SNR first increases then decreases with the rise of D, and a resonance peak appears. This is the classical feature of SR, indicating that the model can generate SR. In Figs. 2–4(b), the vertex has a maximal SNR, where the value of α is less than 1, which indicates that the performance of the asymmetric SR is superior to that of the symmetric SR. In addition, as the asymmetry factor α becomes larger, the optimal noise intensity corresponding to the SNR peak also gradually increases, which means that more noise energy is required to make particle transit between two wells when the well depth is deepened or widened.

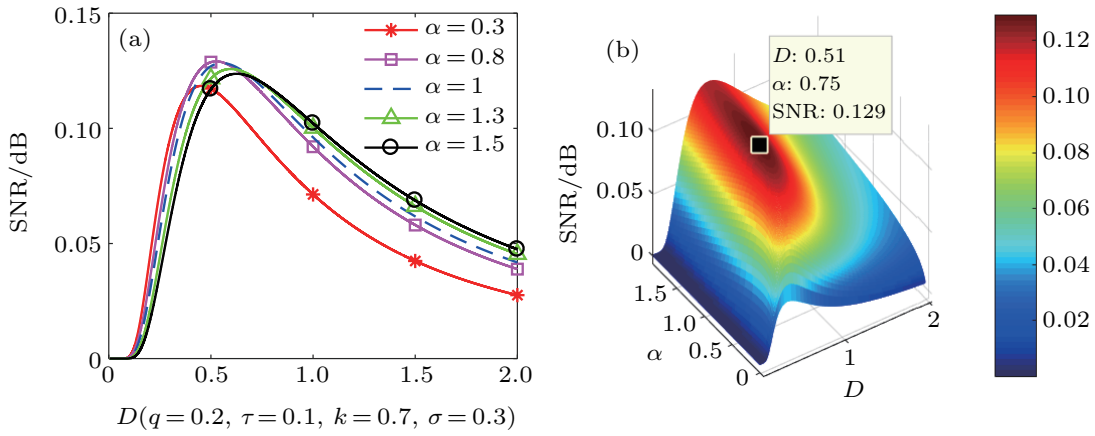


Fig. 2. SNRs changing with D under different α values for DASR where $a = b = 1$ and $A = 0.5$.

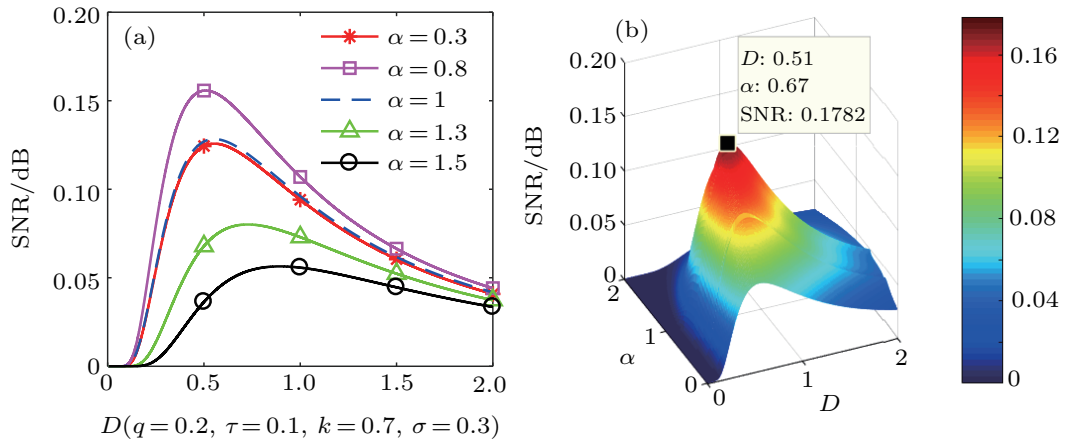


Fig. 3. SNRs changing with D under different α values for WASR where $a = b = 1$ and $A = 0.5$.

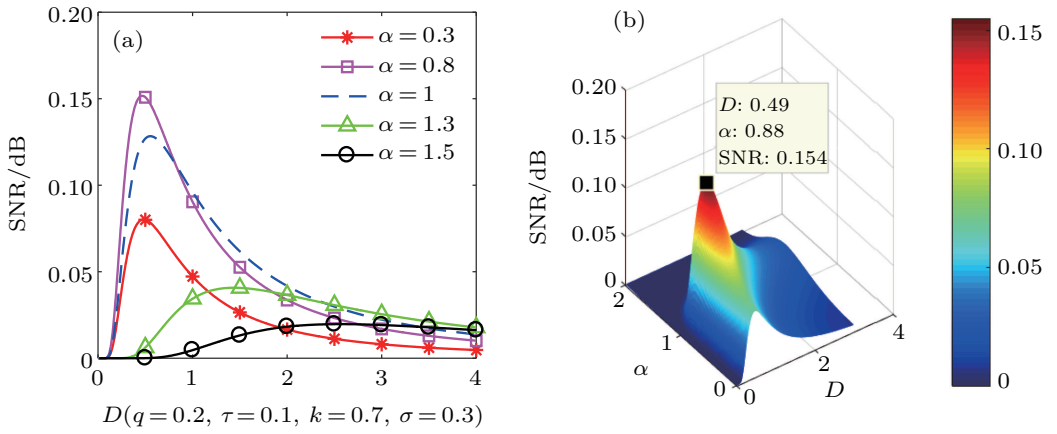


Fig. 4. SNRs changing with D under different α values for DWASR where $a = b = 1$ and $A = 0.5$.

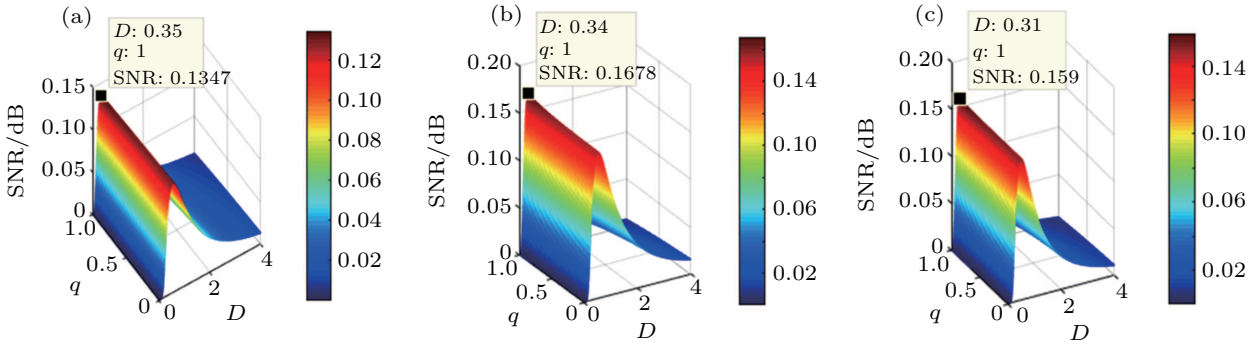


Fig. 5. SNRs changing with D under different q values for (a) DASR, (b) WASR, (c) DWASR where $\alpha = 0.8$, $\tau = 0.1$, $k = 0.7$, $\sigma = 0.3$.

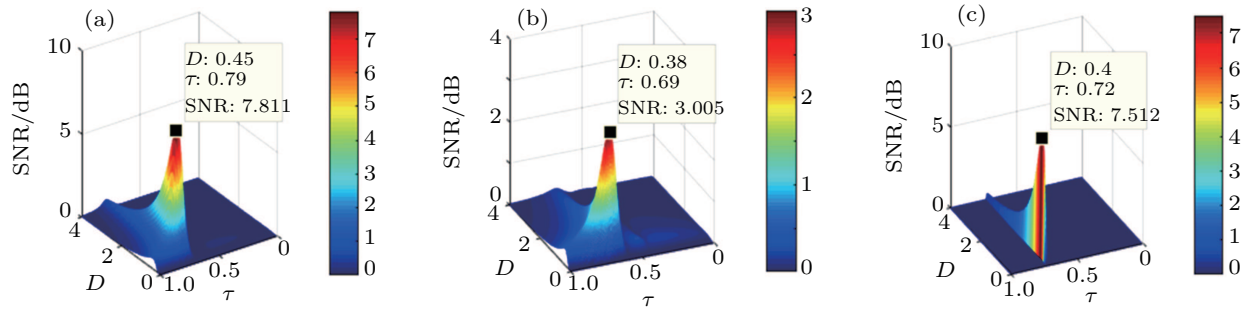


Fig. 6. SNRs changing with D under different τ values for (a) DASR, (b) WASR, (c) DWASR where $\alpha = 0.8$, $q = 0.2$, $k = 0.7$, $\sigma = 0.3$.

Figures 5 and 6 describe the effect of non-Gaussian colored noise on the SNR of DASR, WASR, and DWASR.

The relationship between the SNR and the non-Gaussian noise deviation parameter q is shown in Fig. 5. It is easy to see that the maximum of the SNR is all taken from $q = 1$. When q is 1, the noise has a Gaussian distribution. Therefore, it is considered that the closer to the Gaussian distribution the noise is, the more favorable for the occurrence of SR it is. That is, the Gaussian noise is best. However, the SNR peaks increase slowly with the value of q rising, which proves that it has a small effect on the SNR.

We draw the three-dimensional plots for the SNR which is induced by the correlation time τ in Fig. 6. When $\tau = 0$, the noise is white noise. It is worth mentioning that there is an optimal value of τ that is not 1 to optimize SR effects in Fig. 6. Therefore, colored noise is more conducive to the occurrence of SR than white noise. When τ gradually increases to the optimal value, the SNR peak suddenly rises rapidly and then decreases as τ continues to increase. Comparing with the DWASR, the speeds of decline in the DASR and the WASR are relatively slow. The maximal SNR in Fig. 6(b) is significantly less than that in Figs. 6(a) and 6(c), but it is much higher than that in other figures. The result reveals the truth that the value of the correlation time τ plays a key role in improving the SNR and exciting the SR effect.

Like the non-Gaussian colored noise, we explore the relationship between time-delayed terms and the SNR of DASR, WASR, and DWASR in Figs. 7 and 8.

Figure 7 displays the action of feedback strength k on the SNR in the case that other system parameters are fixed. It can be discovered clearly that there is a maximum of the SNR at $k = 0$, and the increase of feedback strength k causes the SNR peak to decrease rapidly. In other words, there is a negative correlation between the feedback strength k and the SR effect. But beyond that, the feedback strength k represents the degree of dependence of the current state of the system on the past state. The larger the value of k, the stronger the dependency is. These further proves that the enhanced dependency of the SR system on the past state can result in a significant reduction of the resonant peak for the SNR.

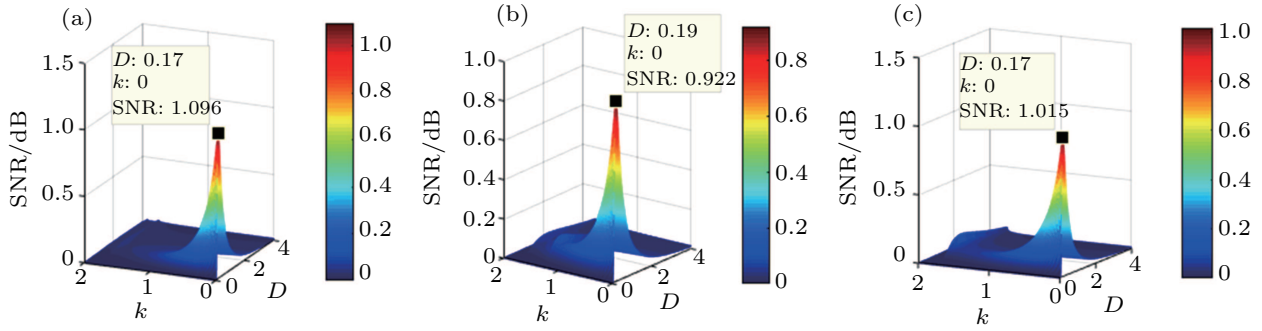


Fig. 7. SNRs changing with D under different k values for (a) DASR, (b) WASR, (c) DWASR where $\alpha = 0.8$, $q = 0.2$, $\tau = 0.1$, $\sigma = 0.3$.

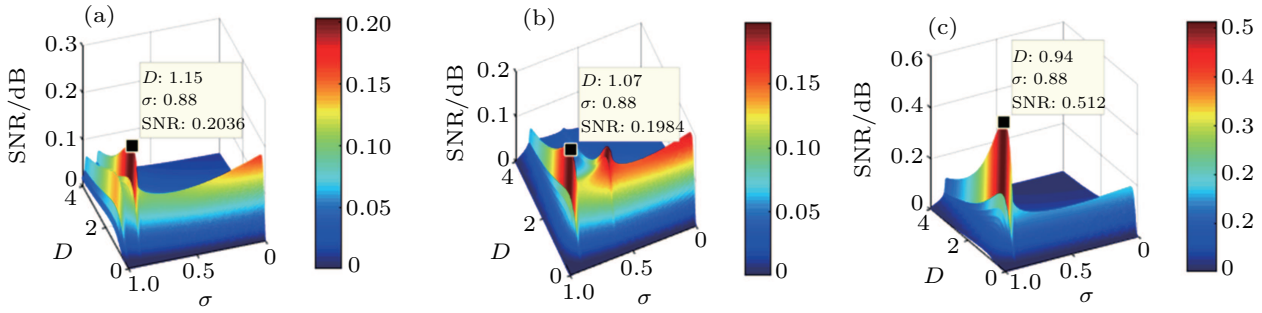


Fig. 8. SNRs changing with D under different σ values for (a) DASR, (b) WASR, (c) DWASR where $\alpha = 0.8$, $q = 0.2$, $\tau = 0.1$, $k = 0.7$.

Figure 8 shows the SNR–D curves of DASR, WASR, and DWASR at different delay time σ values. Unlike the previous three figures, figures 8(a)–8(c) each have two peaks. Hence, the delay time σ and the SNR are not simple monotonic relationships. There are multiple peaks in the influence of the delay time on the SNR, but the optimal σ values corresponding to the maximal SNR all approach to 1. It means that when the time-delayed term is present, the existence of the best σ value makes SR effects the best.

3. SR phenomenon of asymmetric bistable system

3.1. Particle swarm optimization

The inventors of particle swarm optimization algorithm are James Kennedy and Russell Eberhart.[19] This algorithm is developed to imitate the foraging behavior of a flock of birds. The main idea of the algorithm is to use the information shared by individuals in the swarm to obtain an optimal solution.

Particles are used to simulate birds. Each particle can be regarded as an individual searching bird in the search space. The current position of the particle is a candidate solution for the optimization problem. In the meantime, the flight path of the search agent is the individual's search process. There are only two attributes of particles: speed and position. The former represents the speed of movement, and the latter represents the direction of movement. The optimal solution found by the particle is the locally best. The globally best is the optimal value among individual optimal solutions. The updating of speed and position is the main idea of particle swarm algorithm, which can be expressed as

$$\begin{aligned} V_u^{i+1} &= wV_u^i + R_1 r_1 (X_{\text{pu}}^i - X_u^i) + R_2 r_2 (X_{\text{g}}^i - X_u^i), \\ X_u^{i+1} &= X_u^i + V_u^i, \end{aligned} \tag{32}$$

where X_{pu}^i $\left(X_{\text{g}}^i\right)$ is the individual (global) optimal position, w is the inertia coefficient, R_1 and R_2 are the acceleration factors, and r_1 and r_2 are the uniform random numbers generator between 0 and 1.

The algorithm stops when evolution algebra reaches the number of iterations, then returns the final optimal value and the optimal position.

3.2. Weak signal detection of asymmetric bistable system

To analyze the performance of three asymmetric bistable SR systems and prove the superiority of asymmetric systems,

the CSR is chosen for comparison. The steps of weak signal detection are given below.

(i) Signal pre-processing: Set the noise intensity and add noise into the weak signal.

(ii) Frequency scale transformation: Since SR is limited by a small frequency parameter, a frequency scale transformation method is required to achieve SR of high frequency periodic signals.

(iii) Use the particle swarm optimization: Determine the optimal system parameters to maximize SNR by using the particle swarm optimization algorithm.

(iv) Post-processing: Obtain the output signal by using the optimal system parameters and fourth-order Runge–Kutta method. Acquire its waveform and spectrum by Fourier transform and extract weak fault characteristics from the spectrum.

Figure 9 shows the algorithm flowchart.

Figure 10 shows the original cosine signal with a frequency of 0.01, and the noise intensity D of the non-Gaussian colored noise is 3. Figures 10(a) and 10(b) are the original signal without non-Gaussian colored noise, the noise signal with non-Gaussian colored noise, and their spectra. It can be seen that the original signal is difficult to observe under the influence of noise. The input SNR is -38.2194 dB. Figures 10(c)–10(f) are the output signals and their spectra processed by CSR, DASR, WASR, and DWASR. The optimal parameters of CSR are $a = 1$ and $b = 1$, and the SNR is -24.0892 dB.

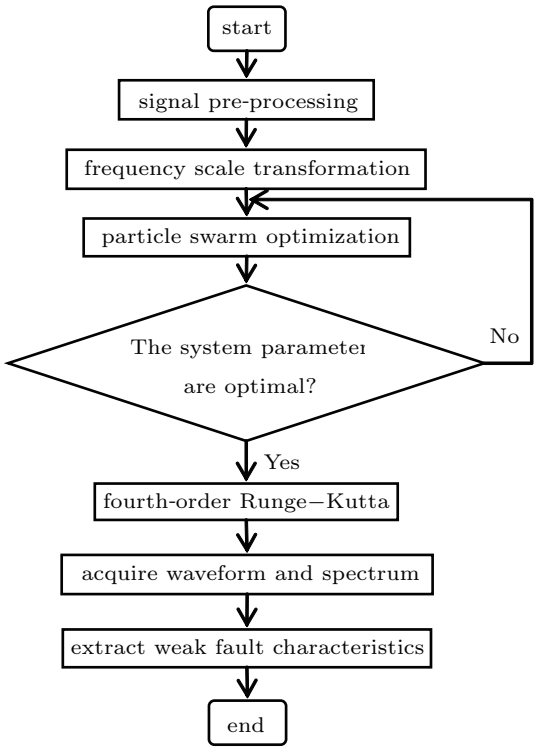


Fig. 9. Flow chart of weak signal detection.

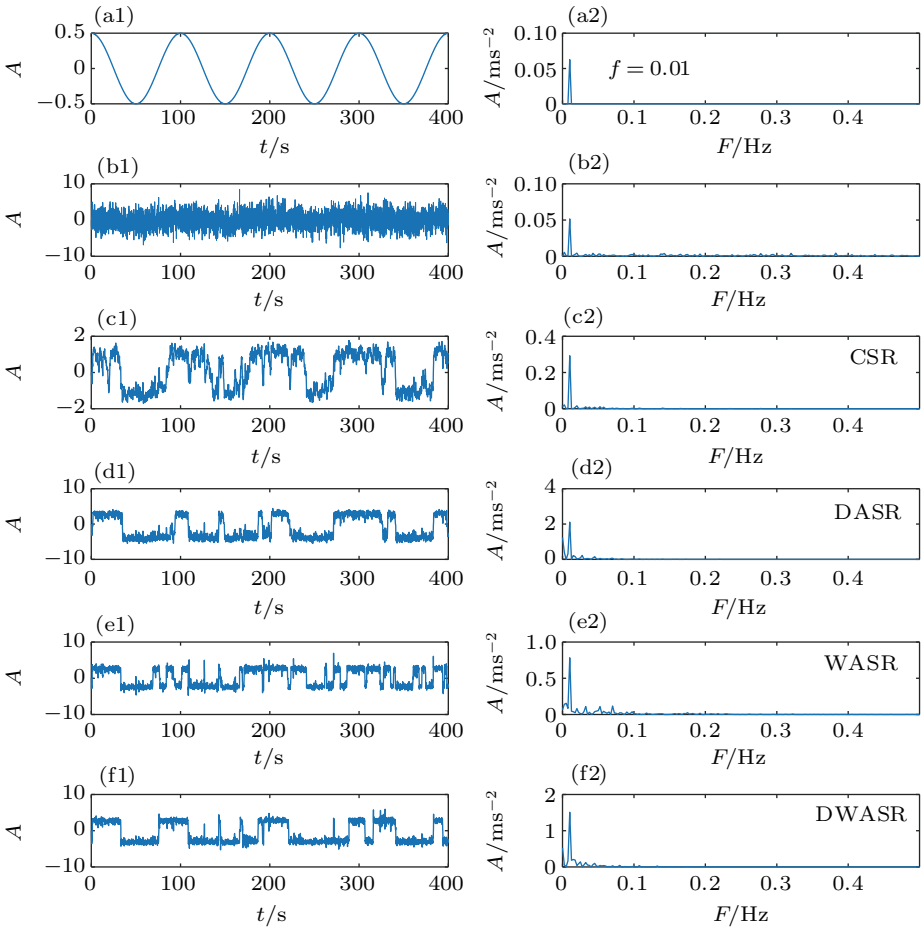


Fig. 10. (a) Original cosine signal and spectrum, (b) noise-added signal and its spectrum, and (c)–(f) output signal with spectra processed by CSR, DASR, WASR, and DWASR, respectively, when $f = 0.01$ and $D = 3$.

The spectrum of the noise-added signal after CSR processing is shown in Fig. 10(c). Meanwhile, the output signal and its spectrum are shown in Figs. 10(d)–10(f). The optimal parameters of the three asymmetric stochastic resonance systems are obtained by the particle swarm optimization algorithm, so that the output SNRs of DASR with $(a,b) = (0.38, 0.14)$, WASR with $(a,b) = (0.85, 0.24)$, and DWASR with $(a,b) = (0.8, 0.19)$ are -12.1904 dB, -15.3832 dB, -13.8027 dB, respectively. The result shows that the three asymmetric systems and the CSR can effectively detect the original signal, where the DASR is the best, the DWASR is the second, and the WASR is the worst. However, they are superior to the CSR, which proves the accuracy of the previous analysis of the asymmetry ratio parameter.

In order to verify the universality of the asymmetric system and the capability for detecting weak signals under strong noise background, a signal with a frequency of 400 Hz and a noise intensity D of 8 is taken as the input signal. The output signal obtained by processing the input signal through the SR system is shown in Fig. 11. The parameters are set to be as follows: $(a,b) = (1,1)$ in the CSR, $(a,b,\alpha) = (0.4992, 0.0268, 0.8077)$ in the DASR, $(a,b,\alpha) = (0.2368, 0.0184, 0.8007)$ in the WASR, and $(a,b,\alpha) = (0.542, 0.0267, 0.8424)$ in the DWASR. Subsequently, the noise-added signals processed by the CSR, DASR, WASR, and DWASR are shown in Figs. 11(c)–11(f). Output SNRs of different types of SR are listed in Table 1. The analysis result is similar to the scenario Fig. 10. Even if the characteristics of the high frequency periodic signal are more difficult to observe due to the increase of the noise intensity, they are still detected after the processing of the SR system. As the results show, the asymmetric SR system can effectively detect the high frequency signal with strong noise, and is better than the symmetric SR system.

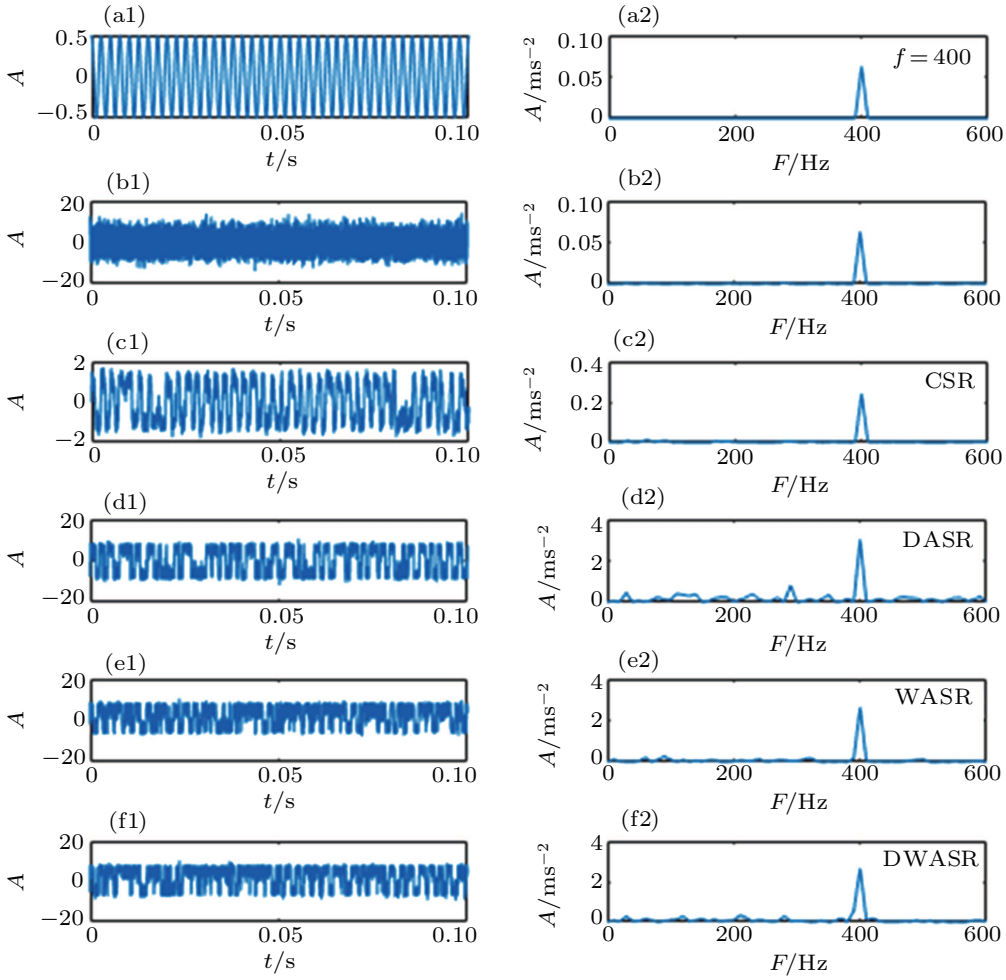


Fig. 11. (a) Original cosine signal and spectrum, (b) noise-added signal and its spectrum, and (c)–(f) output signal with spectra processed by CSR, DASR, WASR, and DWASR, respectively, when $f = 400$ and $D = 8$.

Table 1. Performance of different methods in processing kinds of noise-added signals.

Noise-added signal	Input SNR/dB	Output SNR/dB			
		CSR	DASR	WASR	DWASR
$f = 0.01$ and $D = 3$	-38.2194	-24.0892	-12.1904	-15.3832	-13.8027
$f = 400$ and $D = 8$	-45.4287	-26.4984	-11.703	-19.6365	-14.5029

4. Conclusions

In nature, the time lag is widespread, and the noise is colored. Therefore, it is of great significance to study the asymmetric SR under the influence of the time-delayed feedback and the non-Gaussian colored noise. The output SNR of the model is calculated and the effects of the time-delayed feedback and the non-Gaussian colored noise on the asymmetric SR are analyzed. The results show that the asymmetric SR is superior to that of the symmetric SR. Under the action of the non-Gaussian colored noise, the best performance of SR is derived from the Gaussian-distributed noise while different values of the non-Gaussian noise deviation parameter have little effect on performance. At the same time, in comparison with the white noise, the colored noise is meaningful and plays a crucial role in motivating the SR phenomenon. On the contrary, the time-delayed term reduces the resonant peak for the SNR rapidly and weakens the SR effect. When the time lag exists, there is an optimal delay time σ approaching to 1 to maximize the performance of the SR. From the spectrum analyses of three asymmetric systems, we can find that the best SR is the DASR, the second best SR is the DWASR, and the worst SR is the WASR. At the same time, the asymmetric system performance is better than the symmetric systems. It is worth mentioning that under the background of the strong noise, the three asymmetric SR systems can effectively detect the weak signals, including high-frequency signals.

Appendix A

In the general potential function $\psi(x)$, some lengthy coefficients are listed as follows:

$$
\begin{aligned}
z_1 &= 2b^2\tau_0 x^6 + (1-4a\tau_0 + k(1-4\tau_0))\, bx^4,\\
z_2 &= 3a\tau_0(a\tau_0 - k\sigma + 2k\tau_0 - 1)\\
&\quad + k^2\left(\sigma^2 - 3\sigma\tau_0 + 3\tau_0^2\right)x^2,\\
z_3 &= k^2\sigma^2(1-k\sigma+2k\tau_0+2a\tau_0)\\
&\quad \times \ln\left(3b\tau_0 x^2 - a\tau_0 - k\sigma - k\tau_0 + 1\right),\\
z_4 &= x\left(1 + b\tau_0 x^2 + k\sigma - \tau_0(a+k)\right),\\
z_5 &= \begin{cases} \dfrac{k^2\sigma^2 \operatorname{atan}\left(\dfrac{\sqrt{3b\tau_0}x}{\sqrt{C_\mathrm{b}}}\right)}{\sqrt{3b\tau_0 C_\mathrm{b}}}, & C_\mathrm{b} \geqslant 0,\\ \dfrac{k^2\sigma^2 \ln\left(\dfrac{3b\tau_0 x - \sqrt{-3b\tau_0 C_\mathrm{b}}}{3b\tau_0 x + \sqrt{-3b\tau_0 C_\mathrm{b}}}\right)}{2\sqrt{-3b\tau_0 C_\mathrm{b}}}, & C_\mathrm{b} < 0, \end{cases}\\
C_\mathrm{b} &= 1 - k\sigma - k\tau_0 - a\tau_0,\\
z_6 &= \ln\left|\frac{\sqrt{D_0}\left(1 + \dfrac{k\sigma}{\tau_0(a-3bx^2+k)-1}\right)}{\tau_0(a-3bx^2+k)-1}\right|,
\end{aligned}
$$

$$
\begin{aligned}
j_1 &= 2b^2B_i^2\tau_0 x^6 + (1-4aA_i\tau_0 + k(1-4\tau_0))\, bB_i x^4,\\
j_2 &= 3aA_i\tau_0(aA_i\tau_0 - k\sigma + 2k\tau_0 - 1)\\
&\quad + k^2\left(\sigma^2 - 3\sigma\tau_0 + 3\tau_0^2\right)x^2,\\
j_3 &= k^2\sigma^2(1-k\sigma+2k\tau_0+2aA_i\tau_0)\\
&\quad \times \ln\left(3bB_i\tau_0 x^2 - aA_i\tau_0 - k\sigma - k\tau_0 + 1\right),\\
j_4 &= x\left(1 + bB_i\tau_0 x^2 + k\sigma - \tau_0(aA_i+k)\right),\\
j_5 &= \begin{cases} \dfrac{k^2\sigma^2 \operatorname{atan}\left(\dfrac{\sqrt{3bB_i\tau_0}x}{\sqrt{C_\mathrm{d}}}\right)}{\sqrt{3bB_i\tau_0 C_\mathrm{d}}}, & C_\mathrm{d} \geqslant 0,\\ \dfrac{k^2\sigma^2 \ln\left(\dfrac{3bB_i\tau_0 x - \sqrt{-3bB_i\tau_0 C_\mathrm{d}}}{3bB_i\tau_0 x + \sqrt{-3bB_i\tau_0 C_\mathrm{d}}}\right)}{2\sqrt{-3bB_i\tau_0 C_\mathrm{d}}}, & C_\mathrm{d} < 0, \end{cases}\\
C_\mathrm{d} &= 1 - k\sigma - k\tau_0 - aA_i\tau_0,\\
j_6 &= \ln\left|\frac{\sqrt{D_0}\left(1 + \dfrac{k\sigma}{\tau_0(aA_i-3bB_ix^2+k)-1}\right)}{\tau_0(aA_i-3bB_ix^2+k)-1}\right|.
\end{aligned}
$$

The coefficients c_1–c_6 and e_1–e_6 derived from the transition rates $W_\pm(t)$ are expressed as follows:

$$
\begin{aligned}
c_1 &= \frac{a^3\tau(3q-5)}{4Db(q-2)} + \frac{a^2(3q-5)^2(1+k\sigma)}{16Db(q-2)^2}\\
&\quad + \frac{8a^2\tau(3q-5)(2-q)(a+k)}{16Db(q-2)^2},\\
c_2 &= \frac{a(3q-5)}{48Db(q-2)^3}C_\mathrm{e},\\
C_\mathrm{e} &= -3\tau^2(2a+k)^2(q-2)^2\\
&\quad + 6\tau(3q-5)(q-2)(k+a(k\sigma+1))\\
&\quad - k^2(3q(\sigma-\tau)-5\sigma+6\tau)^2,\\
c_3 &= k^2\sigma^2(3q-5)^4(1-k\sigma)C_\mathrm{f}\\
&\quad + 4\tau k^2\sigma^2(3q-5)^4(a+k)(q-2)C_\mathrm{f},\\
C_\mathrm{f} &= \frac{\ln\left(\dfrac{(3q-5)(1-k\sigma)+2\tau(2-q)(a+k)}{2\tau(2a-k)(q-2)+(1-k\sigma)(3q-5)}\right)}{288Db\tau^2(q-2)^4},\\
c_4 &= \frac{\ln\left(\left|\dfrac{C_\mathrm{g}\left(\dfrac{k\sigma}{C_\mathrm{h}}+1\right)}{C_\mathrm{h}\left(\dfrac{k\sigma}{C_\mathrm{g}}-1\right)}\right|^4\right)}{4(3q-5)^2},\\
C_\mathrm{g} &= \frac{\tau(2q-4)(2a-k)}{3q-5} + 1,\\
C_\mathrm{h} &= \frac{\tau(a+k)(2q-4)}{3q-5} - 1,\\
c_5 &= \sqrt{\frac{a}{b}}\left(\frac{(3q-5)^2(1+k\sigma)}{4D(q-2)^2} - \frac{k\tau(3q-5)}{2D(q-2)}\right),
\end{aligned}
$$

$$c_6 = \begin{cases} \dfrac{k^2\sigma^2 \operatorname{atan}\left(\dfrac{\sqrt{C_\mathrm{k}}}{\sqrt{C_\mathrm{j}}}\right)}{\sqrt{C_\mathrm{k}C_\mathrm{j}}}, & C_\mathrm{j} \geqslant 0, \\ \dfrac{k^2\sigma^2 \ln\left(\dfrac{C_\mathrm{k}\sqrt{\dfrac{a}{b}} - \sqrt{-C_\mathrm{k}C_\mathrm{j}}}{C_\mathrm{k}\sqrt{\dfrac{a}{b}} + \sqrt{-C_\mathrm{k}C_\mathrm{j}}}\right)}{2\sqrt{-C_\mathrm{k}C_\mathrm{j}}}, & C_\mathrm{j} < 0, \end{cases}$$

$$C_\mathrm{j} = 1 - \frac{\tau(a+k)(2q-4)}{3q-5} - k\sigma,$$

$$C_\mathrm{k} = \frac{3b\tau(2q-4)}{3q-5},$$

$$e_1 = \frac{a^2A_i^2(3q-5)^2(1+k\sigma)}{16DbB_i(q-2)^2} + \frac{a^2A_i^2\tau(3q-5)(aA_i - 2\tau(aA_i+k))}{4DbB_i(q-2)},$$

$$e_2 = \frac{aA_i(3q-5)}{48DbB_i(q-2)^3}C_\mathrm{m},$$

$$C_\mathrm{m} = -3\tau^2(2aA_i+k)^2(q-2)^2 + 6\tau(3q-5)(q-2)(k+aA_i(k\sigma+1)) - k^2(3q(\sigma-\tau)-5\sigma+6\tau)^2,$$

$$e_3 = k^2\sigma^2(3q-5)^4(1-k\sigma)C_\mathrm{n} + 4\tau k^2\sigma^2(3q-5)^4(aA_i+k)(q-2)C_\mathrm{n},$$

$$C_\mathrm{n} = \frac{\ln\left(\dfrac{(3q-5)(1-k\sigma)+2\tau(2-q)(aA_i+k)}{2\tau(2aA_i-k)(q-2)+(1-k\sigma)(3q-5)}\right)}{288DbB_i\tau^2(q-2)^4},$$

$$e_4 = \frac{\ln\left(\left|\dfrac{C_\mathrm{o}\left(\dfrac{k\sigma}{C_\mathrm{p}}+1\right)}{C_\mathrm{p}\left(\dfrac{k\sigma}{C_\mathrm{o}}-1\right)}\right|^4\right)}{4(3q-5)^2},$$

$$C_\mathrm{o} = \frac{\tau(2q-4)(2aA_i-k)}{3q-5} + 1,$$

$$C_\mathrm{p} = \frac{\tau(aA_i+k)(2q-4)}{3q-5} - 1,$$

$$e_5 = \sqrt{\frac{aA_i}{bB_i}}\left(\frac{(3q-5)(1+k\sigma)+2k\tau(2-q)}{3q-5}\right),$$

$$e_6 = \begin{cases} \dfrac{k^2\sigma^2 \operatorname{atan}\left(\dfrac{\sqrt{C_\mathrm{r}}}{\sqrt{C_\mathrm{q}}}\right)}{\sqrt{C_\mathrm{r}C_\mathrm{q}}}, & C_\mathrm{q} \geqslant 0, \\ \dfrac{k^2\sigma^2 \ln\left(\dfrac{C_\mathrm{r}\sqrt{\dfrac{aA_i}{bB_i}} - \sqrt{-C_\mathrm{r}C_\mathrm{q}}}{C_\mathrm{r}\sqrt{\dfrac{aA_i}{bB_i}} + \sqrt{-C_\mathrm{r}C_\mathrm{q}}}\right)}{2\sqrt{-C_\mathrm{r}C_\mathrm{q}}}, & C_\mathrm{q} < 0, \end{cases}$$

$$C_\mathrm{q} = 1 - \frac{\tau(aA_i+k)(2q-4)}{3q-5} - k\sigma,$$

$$C_\mathrm{r} = \frac{3bB_i\tau(2q-4)}{3q-5}.$$

References

[1] Liu W H, Sun K H and He S B 2017 *Nonlinear Dyn.* **89** 2521

[2] Li C J, Xu X M, Ding Y P, Yin L Z and Dou B B 2018 *Int. J. Mod. Phys. B* **32** 1850103

[3] Wu J J, Leng Y G, Qiao H, Liu J J and Zhang Y Y 2018 *Acta Phys. Sin.* **67** 210502 (in Chinese)

[4] Jin Y F 2018 *Chin. Phys. B* **27** 050501

[5] Peng H H, Xu X M, Yang B C and Yin L Z 2016 *J. Phys. Soc. Jpn.* **85** 044005

[6] Benzi R, Sutera A and Vulpiani A 1981 *J. Phys. A: Math. Gen.* **14** L453

[7] Strier E, Germán Drazer and Wio H S 2000 *Physica A* **283** 255

[8] Evstigneev M, Reimann P, Pankov V and Prince R H 2004 *Europhys. Lett.* **65** 7

[9] Agudov N V, Krichigin A V, Valenti D and Spagnolo B 2010 *Phys. Rev. E* **81** 051123

[10] Lin L and Duan W L 2015 *Physica A* **427** 155

[11] Li Q Q, Xu X M, Yin L Z, Ding Y P, Ding J F and Sun K H 2018 *Chin. Phys. B* **27** 034203

[12] Li H T, Qin W Y, Lan C B, Deng W Z and Zhou Z Y 2016 *Smart Mater. Struct.* **25** 015001

[13] Wang J and Ning L G 2018 *Chin. Phys. B* **27** 010501

[14] Zhang X H and Liu S Q 2018 *Chin. Phys. B* **27** 040501

[15] Wang S and Wang F Z 2018 *Acta Phys. Sin.* **67** 160502 (in Chinese)

[16] Wio H S and Bouzat S 1999 *Braz. J. Phys.* **29** 136

[17] Li J H 2002 *Phys. Rev. E* **66** 031104

[18] Fuentes M A, Toral R and Wio H S 2001 *Physica A* **295** 114

[19] Fuentes M A, Wio H S and Toral R 2002 *Physica A* **303** 91

[20] Mei D C, Xie G Z, Cao L Y and Wu D J 1999 *Phys. Rev. E* **59** 3880

[21] Mei D C, Xie C W and Zhang L 2003 *Phys. Rev. E* **68** 051102

[22] Jia Y and Li J R 1998 *Physica A* **252** 417

[23] Jin Y F and Xu W 2005 *Chaos Solitons Fractals.* **23** 275

[24] Cao L, Wu D J and Ke S Z 1995 *Phys. Rev. E* **52** 3228

[25] Wang C J, Yang K L and Du C Y 2017 *Physica A* **470** 261

[26] Dybiec B and Gudowska-Nowak E 2006 *Acta Phys. Pol. B* **37** 1479

[27] Liu J, Cao J, Wang Y G and Hu B 2019 *Physica A* **517** 321

[28] Shi P M, Xia H F, Han D Y and Fu R R 2017 *Chin. J. Phys.* **55** 133

[29] Feng Y L, Dong J M, Tang X L 2016 *Chin. Phys. Lett.* **33** 108701

[30] Tang J C, Shi B Q and Li Z X 2018 *Chin. J. Phys.* **56** 2104

[31] Liu J and Wang Y G 2018 *Physica A* **493** 359

[32] Tan H, Liang X S, Wu Z Y, Wu Y K and Tan H C 2019 *Chin. J. Phys.* **57** 362

[33] Luo J J, Xu X M, Ding Y P, Yang B C, Yuan Y B, Sun K H and Yin L Z 2018 *Eur. Phys. J. Plus* **133** 239

[34] Li M P, Xu X M, Yang B C and Ding J F 2015 *Chin. Phys. B* **24** 060504

[35] Zhao Y, Xu W, Zou S C 2009 *Acta Phys. Sin.* **58** 1396 (in Chinese)

[36] Guillouzic S, L'Heureux I and Longtin A 1999 *Phys. Rev. E* **59** 3970

[37] Yang T, Liu R F, Zeng C H and Duan W L 2017 *Chin. J. Phys.* **55** 275

[38] Kennedy J and Eberhart R 1995 *Proceedings of the IEEE International Conference on Neural Networks* November 27–December 1, 1995, Perth, Australia, p. 1942